Mesoporous Catalysts Hot Paper

International Edition: DOI: 10.1002/anie.201502892
German Edition: DOI: 10.1002/ange.201502892

Ligand-Assisted Co-Assembly Approach toward Mesoporous Hybrid Catalysts of Transition-Metal Oxides and Noble Metals: Photochemical Water Splitting**

Ben Liu, Chung-Hao Kuo, Jiejie Chen, Zhu Luo, Srinivas Thanneeru, Weikun Li, Wenqiao Song, Sourav Biswas, Steven L. Suib, and Jie He**

Abstract: *A bottom-up synthetic approach was developed for the preparation of mesoporous transition-metal-oxide/noble-metal hybrid catalysts through ligand-assisted co-assembly of amphiphilic block-copolymer micelles and polymer-tethered noble-metal nanoparticles (NPs). The synthetic approach offers a general and straightforward method to precisely tune the sizes and loadings of noble-metal NPs in metal oxides. This system thus provides a solid platform to clearly understand the role of noble-metal NPs in photochemical water splitting. The presence of trace amounts of metal NPs (≈0.1 wt%) can enhance the photocatalytic activity for water splitting up to a factor of four. The findings can conceivably be applied to other semiconductors/noble-metal catalysts, which may stand out as a new methodology to build highly efficient solar energy conversion systems.*

The current studies on the design of efficient systems for the conversion of solar energy through photochemical water splitting are mainly devoted to two important issues, 1) the energy capture, that is, how to sufficiently absorb photons in the solar energy spectrum, and 2) the charge separation, that is, how to effectively avoid the recombination of excitons and to maximally utilize the excitons.[1] Among a variety of semiconducting catalysts, inexpensive and non-photocorrosive transition-metal oxides (e.g. TiO_2, CeO_2, and WO_3) are excellent candidates for photochemical water splitting. Unfortunately, all these semiconducting materials have a large band gap,[2] resulting in a low utilization of solar energy in the visible and near-infrared range of 400–1000 nm, in which approximately 60% of the solar energy lies. One solution is to make use of noble-metal nanoparticles (NPs; e.g. Au and Ag) as photoantennas to sensitize catalytic materials.[3] However, the role of noble-metal NPs in photochemical water splitting has been debated in a number of recent reports.[3c–j] Murdoch et al. demonstrated that the photocatalytic activity of hybrid catalysts of TiO_2/AuNPs increased proportionally with the loading of AuNPs (up to 4 wt%), while the size of AuNPs in the range of 3–12 nm did not affect the rate of photocatalytic hydrogen production.[4] Meanwhile, other recent reports showed that 1) heavy loading and non-uniform distributions of noble-metal NPs in metal oxides may increase the recombination of excitons, thus leading to the decrease of photocatalytic activity,[3d,5] and 2) varying the size of AuNPs can change the efficiency of hot electron injection.[3e,6] These conflicting observations on the role of noble-metal NPs in photochemical water splitting are likely due to the poor controllability in the topological distribution and size dispersity of noble-metal NPs in hybrid catalysts. The large polydispersity of these NPs can distort the differences in catalytic activity that may stem from the change of NP sizes and loadings. Given the current synthetic approaches, including physical mixing[7] and in situ photo- or chemical reduction,[5a,8] none of them can directly control the size, loading, and distribution of noble-metal NPs in metal oxide catalysts. Thus, a novel and general platform of hybrid catalysts is urgently needed to better understand the role of noble-metal NPs in photochemical water splitting.

We herein report a bottom-up synthetic approach to engineer the nanostructure of mesoporous hybrid catalysts of transition-metal oxides and noble metals and to study the role of noble-metal NPs in photochemical water splitting. Figure 1a schematically illustrates our design principle and the synthetic route toward the hybrid catalysts. This approach combines the use of amphiphilic block-copolymer (BCP) micelles and polymer-tethered noble-metal NPs as co-structure-directing surfactants to prepare hybrid mesoporous catalysts. Basically, in the presence of transition-metal precursors, the co-assembly of two structure-directing surfactants creates a three-dimensional artificial scaffold followed by the sol–gel processes of transition-metal oxides.[9] The polymer-tethered noble-metal NPs with a similar chemical composition of polymer micelles could 1) uniformly distribute in metal oxides without disturbing their intrinsic ordered

[*] Dr. B. Liu, C.-H. Kuo, S. Thanneeru, Dr. W. Li, W. Song, S. Biswas, Prof. S. L. Suib, Prof. J. He
Department of Chemistry, University of Connecticut
Storrs, CT 06269 (USA)
E-mail: steven.suib@uconn.edu
jie.he@uconn.edu
Z. Luo, Prof. S. L. Suib, Prof. J. He
Institute of Material Science, University of Connecticut
Storrs, CT 06269 (USA)
J. Chen
Department of Chemistry
University of Science & Technology of China
Hefei 230026 (China)

[**] J.H. is grateful for the financial support of startup funds from the University of Connecticut. S.L.S. acknowledges support of the US Department of Energy, Office of Basic Energy Sciences, Division of Chemical, Biological and Geological Sciences under grant DE-FG02-86ER13622A000. The authors thank Yan Xia for her assistance on SAXS measurement. This work was also partially supported by the Green Emulsions Micelles and Surfactants (GEMS) Center.

Supporting information for this article is available on the WWW under http://dx.doi.org/10.1002/anie.201502892.

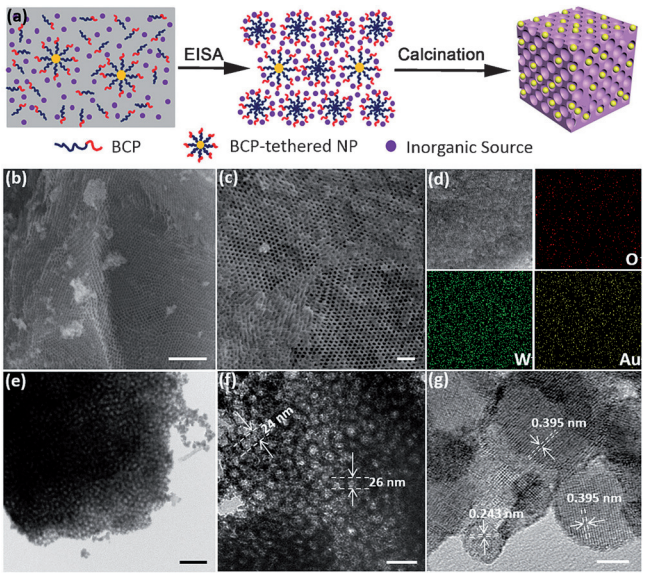

Figure 1. a) Synthesis of mWO$_3$/AuNP hybrid catalysts. b,c) SEM images of mWO$_3$/AuNP-8(0.1%), indicating highly ordered mesostructures. d) SEM-EDX mapping of mWO$_3$/AuNP-8(0.1%), showing the homogeneous distribution of O (red), W (green), and Au (yellow). e–g) TEM images of mWO$_3$/AuNP-8(0.1%). Scale bars in b, c, e, f, and g represent 500, 200, 200, 100, and 5 nm, respectively.

mesoporous structure, and 2) preserve the size uniformity of noble-metal NPs. Our synthetic approach therefore offers a general and straightforward method to hybrid catalysts with aggregation-free and thermally stable noble-metal NPs. The obtained hybrid catalysts provide a platform to clearly determine the role of noble-metal NPs in photochemical water splitting.

As a prototype system, we used an amphiphilic BCP of poly(ethylene oxide)-*block*-polystyrene (PEO_{114}-*b*-PS_{223}) and AuNPs tethered by PEO_{45}-*b*-PS_{267}-SH (AuNP-PS-*b*-PEO) as co-structure-directing surfactants to prepare mesoporous tungsten oxide (mWO$_3$)/AuNP hybrid catalysts. In a typical synthesis, the predetermined amounts of the surfactants of PEO-*b*-PS and AuNP-PS-*b*-PEO and tungsten precursors of WCl_6 were first mixed in THF. A small amount of concentrated HCl was added to adjust the coordination interaction between PEO blocks and W ions. After the removal of solvent by evaporation, the film was calcined at 500 °C for 4 h to give hybrid, dark-yellow mWO$_3$/AuNP catalysts (see the Supporting Information for synthetic details). The mWO$_3$ catalysts with various sizes and loadings of AuNPs are denoted as mWO$_3$/AuNP-*D*-(*A*%), hereafter, in which *D* is the average diameter of AuNPs in nanometers and *A*% is the weight percentage of AuNPs relative to WO$_3$, respectively.

The obtained mWO$_3$/AuNP hybrid catalysts were carefully characterized by field emission scanning electron microscopy (FESEM), transmission electron microscopy (TEM), and small-angle X-ray scattering (SAXS). The FESEM (Figure 1 b,c) and TEM (Figure 1 e,f) images of mWO$_3$/AuNP-8(0.1%) show that the calcined catalyst possesses long-range, periodically ordered mesoporous nanostructures. The nearly defect-free pores of mWO$_3$/AuNP-8(0.1%) are rather uniform throughout and the average pore size is approximately 25 nm with a wall thickness of 18 nm. The SEM energy-dispersive X-ray (SEM-EDX) mapping image (Figure 1 d) and dark-field TEM images (Figure S3 in the Supporting Information) indicate the W, O, and Au elements are homogeneously distributed through the entire area. The high-resolution TEM image of mWO$_3$/AuNP-8(0.1%) confirms a crystalline framework of mesoporous WO$_3$ (Figure 1 g). The lattice fringe of Au (111) plane with *d*-spacing of 0.24 nm and WO$_3$ (002) plane with *d*-spacing of 0.39 nm can be clearly observed after calcination. Furthermore, the SAXS pattern of mWO$_3$/AuNP-8(0.1%) shows well-resolved (111), (311), and (500) reflections, confirming an ordered face-centered cubic (*fcc*) mesostructure with the space group $Fm\bar{3}m$ (Figure 2 a). The cell parameter (*d*-spacing) was calculated to be approximately 44 nm, in good agreement with SEM and TEM results. The Brunauer–Emmett–Teller (BET) specific surface area of the mWO$_3$/AuNP-8(0.1%) catalyst was estimated to be 70.4 $m^2 g^{-1}$ with a pore size of 21.7 nm (Figure S4).

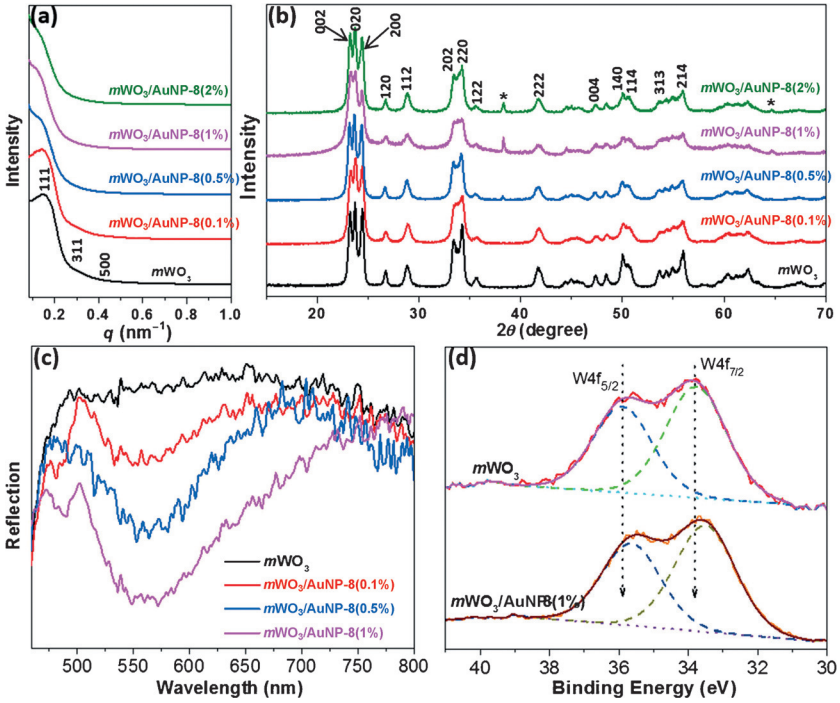

Figure 2. Structural characterizations of mWO$_3$/AuNP-8 hybrid catalysts. a) SAXS and b) XRD patterns of mWO$_3$/AuNP-8 catalysts with various loadings of AuNPs. The diffraction peaks denoted with * in (b) are attributed to gold (111) and (220) facets. c) UV/Vis diffuse reflectance spectra of mWO$_3$/AuNP-8 hybrid catalysts, indicating the surface plasmon absorption peak of AuNPs. d) Evolution of W 4f XPS spectra of mWO$_3$ and mWO$_3$/AuNP-8(1%).

AuNP-PS-*b*-PEO composed of a AuNP core and PS-*b*-PEO tethers, also known as colloidal amphiphiles, is a novel type of colloidal molecule, structurally analogous to spherical micelles of amphiphilic linear BCPs.[10] The utilization of AuNP-PS-*b*-PEO as a co-surfactant is a key to the controllable synthesis of hybrid *m*WO_3/AuNP catalysts. First of all, the BCP tethers improved the stability of AuNPs under the extreme conditions used for the sol–gel process of transition-metal ions, for example an acidic solution with a high ionic strength. In our control experiments, the direct mixing of AuNPs without BCP tethers and tungsten precursors resulted in the immediate aggregation of AuNPs, while no aggregation of AuNP-PS-*b*-PEO was observed under the conditions of the sol–gel process. Second, the polymer tethers played an important role, assisting the co-assembly of amphiphilic BCP micelles and colloidal amphiphiles of AuNPs. Colloidal amphiphiles of AuNP-PS-*b*-PEO essentially have core–shell nanostructures, in which the chemical composition of BCP tethers is identical to that of linear BCP micelles. This avoids the enthalpy-driven immiscibility of two amphiphiles during sol–gel processes, thus ensuring the uniform distribution of AuNPs in the formed oxides. Furthermore, in the course of sol–gel processes that occur within the PEO domain, the pore-forming PS blocks beneath PEO layers limit the mobility of AuNPs. Therefore, only single AuNP can be accommodated in one *fcc* pore after calcination and AuNP fusion or migration does not occur, thus preserving the size and size distribution of AuNPs in these hybrid catalysts (see Figure 3).

The influence of various loadings of AuNPs (0–2%) on the intrinsic long-range ordered mesostructure was further examined by tuning the initial concentration of AuNP-PS-*b*-PEO. The SAXS patterns of calcined *m*WO_3/AuNP-8 are shown in Figure 2a. At a lower AuNP loading (< 0.5%), the well-resolved scattering peaks confirm the conserved mesoporous nanostructures, despite the small shift of the first-order peak (111) toward the low-angle region. The *d*-spacing of the pure *m*WO_3 catalyst without AuNP loading is 42.1 nm, and a gradual increase of *d*-spacing to 46.0 nm for *m*WO_3/AuNP-8(0.5%) was observed with the increase of AuNP loading. However, a further increase of the AuNP loading weakened the intensity of the first-order peak of SAXS patterns, thus indicating a disruption of the long-range order of the mesostructures. The structural transformation to disordered mesoporous nanostructures was found for *m*WO_3/AuNP-8(2%). Because of a slight size mismatch of BCP micelles and AuNP-PS-*b*-PEO colloidal amphiphiles (Figure S2c), the disruption of the ordered assemblies of BCP micelles is expected at a critical concentration of AuNP-PS-*b*-PEO. Similar results were also confirmed from FESEM images (Figures S5–S10). The wide-angle X-ray diffraction (XRD) patterns of *m*WO_3/AuNP-8 (Figure 2b) suggest that all hybrid catalysts possess a monoclinic crystalline phase of WO_3, and no noticeable change in the crystallinity of WO_3 is observed, regardless of the AuNP loading.

In the meantime, the change in visible-light capture of hybrid catalysts can be estimated by UV/Vis diffuse reflectance spectroscopy (DRS; Figure 2c and Figure S11). In the presence of AuNPs, the surface plasmon absorption peaks of hybrid catalysts clearly appeared at 560 nm and the peak intensity increased with the AuNP loading. The surface plasmon resonance of AuNPs is known to be very sensitive to their size and aggregation states.[11] No shift of the absorption peak of AuNPs was observed in DRS spectra. This observation suggests that aggregation of AuNPs did not occur during the sol–gel processes and that the size and homogeneous distribution of the AuNPs in all catalysts are essentially similar.

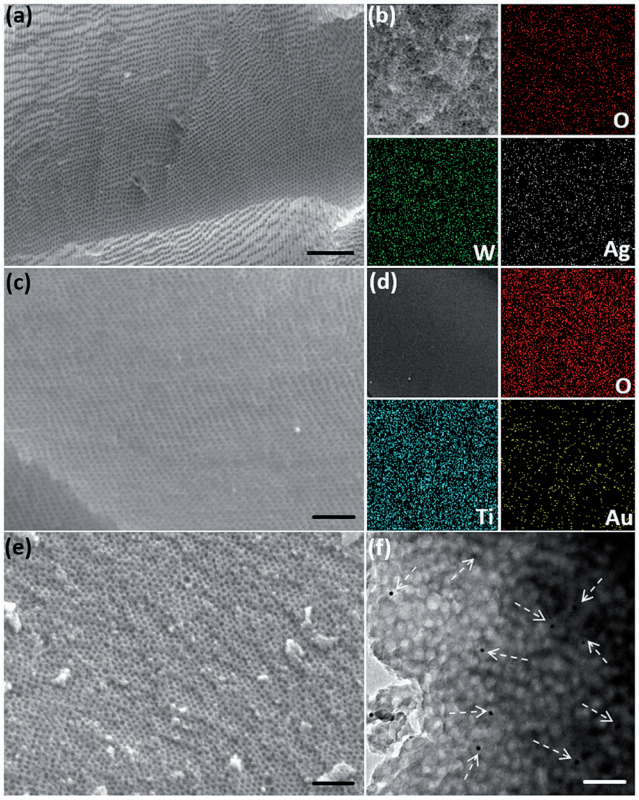

Figure 3. SEM images (a,c,e), SEM-EDX mapping (b,d), and TEM image (f) of the mesoporous hybrid materials of metal (nonmetal) oxides/noble-metal NPs. a,b) *m*WO_3/AgNP-7(0.1%), c,d) *m*TiO_2/AuNP-8(0.1%), and e,f) *m*SiO_2/AuNP-8(0.1%). The arrows in (f) indicate the AuNPs. The scale bars in a, c, e, and f represent 500, 200, 200, and 100 nm, respectively.

X-ray photoelectron spectroscopy (XPS) was further used to characterize the change in surface composition and oxidation state of the hybrid catalysts. The high-resolution XPS spectra of the W 4f region of *m*WO_3/AuNP-8 hybrid catalysts at various loadings of AuNPs are given in Figure 2d. For pure *m*WO_3, two distinct peaks could be fitted as W $4f_{7/2}$ (33.8 eV) and W $4f_{5/2}$ (35.9 eV), corresponding to the difference in binding energy of 2.1 eV, which is in good agreement with reported values of WO_3.[12] This is attributed to W^{6+} species on the surface. The addition of AuNPs clearly resulted in a shift of the W 4f peaks to a lower binding energy (also see Figure S30). In the case of *m*WO_3/AuNP-8(1%), the W $4f_{7/2}$ and W $4f_{5/2}$ peaks were observed at 33.5 eV and 35.6 eV, respectively. The small shift in binding energy of −0.3 eV was attributed to the formation of W species with lower valences, for example, W^{5+} and W^{4+}. This suggests the localized electronic interaction of *m*WO_3 and AuNPs, in which the

presence of partially positive-charged Au^{3+}/Au^{+} compensates for the change of the W valency.

We also examined the effect of various sizes of AuNPs (4–20 nm) on the mesoporous structures of mWO$_3$/AuNP catalysts, as the size mismatch of BCP micelles of PS-*b*-PEO and colloidal amphiphiles of AuNP-PS-*b*-PEO resulted in the competition of ordering during the sol–gel processes. Both SEM and SAXS results indicate that mWO$_3$/AuNP-4-(0.1 %) and mWO$_3$/AuNP-14(0.1 %) possess long-range ordered *fcc* mesoporous structures (Figures S12–S15), similar to that of mWO$_3$/AuNP-8-(0.1 %). Interestingly, the obtained mWO$_3$/AuNP-20(0.1 %) does not contain ordered mesostructures (Figure S15). This result implies that the large size mismatch of two surfactants would eventually disrupt their co-assembly (Figure S2 d). In our current study, the linear BCP of PS-*b*-PEO with a large hydrophobic PS block was chosen to form the larger spherical pore in mWO$_3$ that could accommodate a broad range of AuNPs with various sizes.

Our synthetic methodology can also be applied to prepare other combinations of hybrid catalysts, for example, mWO$_3$/AgNP, mTiO$_2$/AuNP, and mSiO$_2$/AuNP. As shown in Figure 3, all calcined mWO$_3$/AgNP-7(0.1 %), mTiO$_2$/AuNP-8(0.1 %) and mSiO$_2$/AuNP-8 (0.1 %) possess well-ordered mesoporous structures (see Figures S16–S23 for more low magnification TEM/SEM images). The corresponding SEM-EDX mapping images indicate that W (or Ti), O, and Ag (or Au) elements are homogeneously distributed in the entire area. This powerful method may thus give access to a library of mesoporous metal (or nonmetal) oxide/metal NP hybrid materials. In particular, we would like to emphasize that the AuNPs essentially preserved the well-defined size and size distribution in hybrid catalysts. The thermal stability of AuNPs in mesoporous hybrid catalysts also surpasses that of the oxide/AuNP hybrids prepared using traditional physical mixing or in situ reduction methods (Figures S24–S26). Using mSiO$_2$/AuNP as an example (because of the higher TEM contrast), the TEM images and UV/Vis DRS spectra confirm no aggregation or fusion of AuNPs during the calcination up to 12 h at 500 °C (see Figure 3 f, and Figures S21–S23 for more TEM images). In the mesoporous structures of the oxides, the discrete AuNP is accommodated within individual *fcc* pores to avoid the migration and thermal fusion of AuNPs. This also distinguishes our synthetic approach of mesoporous hybrids from the previously reported growth of AuNPs on the surface of metal oxides.

The photocatalytic activity of mWO$_3$/AuNP hybrid catalysts in water oxidation reactions (WORs) was evaluated under irradiation of visible light ($\lambda > 400$ nm) using AgNO$_3$ as a sacrificing electron acceptor. The results of O$_2$ evolution using mWO$_3$/AuNP hybrid catalysts are shown in Figure 4. The nonmesoporous WO$_3$ catalyst without AuNPs (Figure S27) exhibits a poor photocatalytic O$_2$ evolution, as WO$_3$ with a band gap of 2.8 eV has a weak absorption edge of 400 nm. The evolved O$_2$ is 3.0 mmol mol$^{-1}_{W}$ after 4 min, comparable to the reported values.[3d,h] The mesostructured

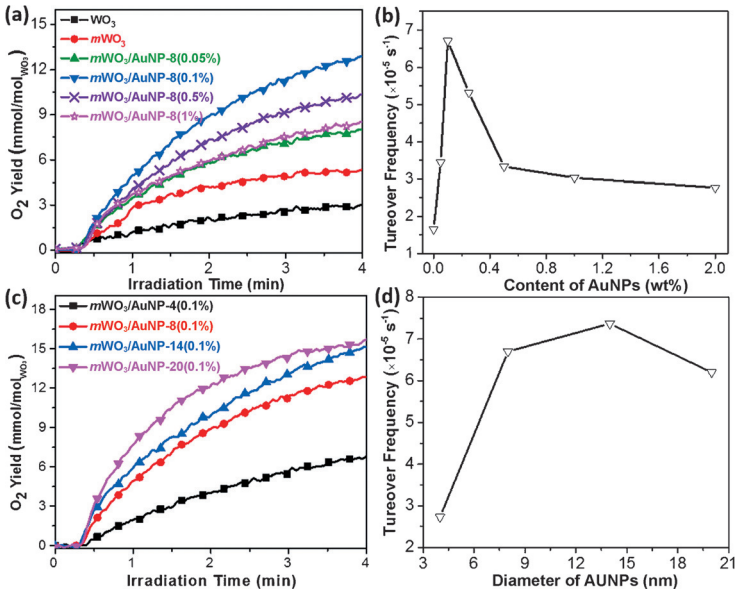

Figure 4. Photocatalytic activity of mWO$_3$/AuNP hybrid catalysts for WORs. (a,c) O$_2$ evolution curves using mWO$_3$/AuNP hybrid catalysts with a) various loadings of AuNPs and c) AuNPs of varying sizes. O$_2$ concentration was recorded by a needle-type oxygen microsensor under visible-light irradiation (>400 nm). Conditions: 2.5 mg of the catalyst in 10 mL of deionized water containing 10 mM of AgNO$_3$ under visible light ($\lambda > 400$ nm). (b,d) Plotting of TOFs of hybrid catalysts as a function of b) the AuNP loading and d) the size of the AuNPs. TOF = turnover frequency.

mWO$_3$ catalyst kinetically enhances the generation rate of O$_2$ as a result of the increase of the surface area. The slope of the O$_2$ evolution curve sharply increases and the turnover frequency (TOF) of mWO$_3$ is 1.65×10^{-5} s^{-1} at 2 min, two times higher than that of the nonmesoporous WO$_3$ catalyst.

A moderate loading of AuNPs in mWO$_3$ catalysts significantly improved the rate of photocatalytic O$_2$ evolution and the amount of produced O$_2$ (see Figure 4 a and Figure S28). For example, the content of dissolved O$_2$ readily increased to 8.0 mmol mol$^{-1}_{W}$ for the mWO$_3$/AuNP-8(0.05 %) and 12.9 mmol mol$^{-1}_{W}$ for the mWO$_3$/AuNP-8(0.1 %) catalyst. The TOF of 6.73×10^{-5} s^{-1} for the mWO$_3$/AuNP-8(0.1 %) catalyst is roughly four times higher than that of the pure mWO$_3$ catalyst (see Table S1). However, a further increase of the AuNP loading seemed to be detrimental for the photocatalytic activity of mWO$_3$. Similar precedents have been reported in TiO$_2$/AuNP[5a] and CeO$_2$/AuNP[3d] catalysts. For comparison, the catalytic activity of mWO$_3$/AuNP hybrid catalysts containing AuNPs of various sizes is also given in Figure 4 c. For mWO$_3$/AuNP-4(0.1 %) with smaller AuNPs, the TOF is 2.7×10^{-5} s^{-1} at 2 min, which is much lower than that of mWO$_3$/AuNP catalysts with larger AuNPs. Nevertheless, in the range of 8–20 nm, the correlation between the reaction rate and the size of the AuNPs seems to be minimal (Figure 4 d).

The incorporation of noble-metal NPs in mesoporous catalysts can maximize the binding of reactants (i.e. water) and catalytic centers as well as shorten the diffusion distance of excitons. This observation further enables to understand the role of AuNPs in mWO$_3$/AuNP hybrid catalysts for WORs. In general, two electron-excitation events are possibly

involved:[13] 1) the band-gap excitation of WO_3, in which the hole generated on the WO_3 frontier HOMO oxidizes water molecules (Figure S31a), and 2) the hot electron injection from AuNPs to the LUMO of WO_3, in which the hole generated in the AuNPs also results in the formation of O_2 (Figure S31b). The higher photocatalytic performance of $m$$WO_3$/AuNP catalysts is presumably a result of the synergetic effect of band-gap excitation of $m$$WO_3$ and hot electron injection of AuNPs. In order to gain more insight into the influence of AuNPs on the reaction pathway and photocatalytic activity, the O_2 evolution was also recorded under $\lambda > 500$ nm irradiation using $m$$WO_3$/AuNP hybrid catalysts. As pure WO_3 does not absorb light of $\lambda > 500$ nm, the excitation of AuNPs would be the sole contribution. However, no significant O_2 production was detected for both $m$$WO_3$ and $m$$WO_3$/AuNP catalysts (Figure S29). Moreover, pure AuNPs were tested for WORs as well and negligible activity was detected. These results strongly suggested that 1) the hot electron injection of AuNPs plays a less important role in the photocatalytic activity of hybrid catalysts (Figure S31b), compared to the band-gap excitation of WO_3, and 2) the enhancement of the photocatalytic activity is likely a result of synergistic effects of $m$$WO_3$/AuNP hybrids as co-catalysts. One possible mechanism is the transfer of photogenerated electrons in WO_3 to AuNPs, leading to an improvement of the oxidation efficiency. This electronic communication between $m$$WO_3$ and AuNPs is also supported by the presence of partially positive-charged Au^{3+}/Au^{+} species, according to XPS results. The similar electron-transfer scenarios at metal/semiconductor interfaces were observed previously in other metal/semiconductor interfaces, for example, AuNP/TiO_2,[5a,6c] Pt/CdSe,[14] and AuNP/MnO_2.[15] At a higher loading of AuNPs, they somehow also act as recombination centers of excitons, thus resulting in a decrease of photocatalytic activity.[3d]

In summary, we demonstrated a general synthetic approach to mesoporous hybrid catalysts of noble metals and transition-metal oxides by utilizing the co-assembly of amphiphilic BCP micelles and colloidal amphiphiles of AuNP-PS-*b*-PEO as co-structure-directing surfactants. The bottom-up synthetic approach constitutes an alternative, general method to engineer the nanostructure of hybrid catalysts with precise control over the loading and size of the noble-metal NPs. The unprecedented photocatalytic activity of $m$$WO_3$/AuNP hybrid catalysts for visible-light-induced WORs was also studied. The presence of trace amounts of AuNPs ($\approx 0.1\,\%$) boosted the photocatalytic activity up to a factor of four, while a decrease of photocatalytic activity was observed at a higher AuNP loading. Our findings can conceivably be applied to other semiconductors/noble-metal catalysts, which may stand out as novel platforms to build highly efficient solar energy conversion systems.

Keywords: mesoporous catalysts · metal nanoparticles · transition-metal oxides · tungsten oxide · water splitting

How to cite: *Angew. Chem. Int. Ed.* **2015**, *54*, 9061–9065
Angew. Chem. **2015**, *127*, 9189–9193

[1] a) J. Yang, D. Wang, H. Han, C. Li, *Acc. Chem. Res.* **2013**, *46*, 1900–1909; b) H. A. Atwater, A. Polman, *Nat. Mater.* **2010**, *9*, 205–213; c) N. Serpone, A. Emeline, *J. Phys. Chem. Lett.* **2012**, *3*, 673–677.
[2] Y. Xu, M. A. Schoonen, *Am. Mineral.* **2000**, *85*, 543–556.
[3] a) S. Linic, P. Christopher, D. B. Ingram, *Nat. Mater.* **2011**, *10*, 911–921; b) K. Awazu, M. Fujimaki, C. Rockstuhl, J. Tominaga, H. Murakami, Y. Ohki, N. Yoshida, T. Watanabe, *J. Am. Chem. Soc.* **2008**, *130*, 1676–1680; c) D. B. Ingram, S. Linic, *J. Am. Chem. Soc.* **2011**, *133*, 5202–5205; d) A. Primo, T. Marino, A. Corma, R. Molinari, H. Garcia, *J. Am. Chem. Soc.* **2011**, *133*, 6930–6933; e) Z. W. Seh, S. Liu, M. Low, S. Y. Zhang, Z. Liu, A. Mlayah, M. Y. Han, *Adv. Mater.* **2012**, *24*, 2310–2314; f) D. Tsukamoto, Y. Shiraishi, Y. Sugano, S. Ichikawa, S. Tanaka, T. Hirai, *J. Am. Chem. Soc.* **2012**, *134*, 6309–6315; g) Z. Bian, T. Tachikawa, P. Zhang, M. Fujitsuka, T. Majima, *J. Am. Chem. Soc.* **2014**, *136*, 458–465; h) A. Tanaka, K. Hashimoto, H. Kominami, *J. Am. Chem. Soc.* **2014**, *136*, 586–589; i) J. B. Joo, R. Dillon, I. Lee, Y. Yin, C. J. Bardeen, F. Zaera, *Proc. Natl. Acad. Sci. USA* **2014**, *111*, 7942–7947; j) J. B. Priebe, M. Karnahl, H. Junge, M. Beller, D. Hollmann, A. Brückner, *Angew. Chem. Int. Ed.* **2013**, *52*, 11420–11424; *Angew. Chem.* **2013**, *125*, 11631–11635.
[4] M. Murdoch, G. Waterhouse, M. Nadeem, J. Metson, M. Keane, R. Howe, J. Llorca, H. Idriss, *Nat. Chem.* **2011**, *3*, 489–492.
[5] a) C. u. Gomes Silva, R. Juárez, T. Marino, R. Molinari, H. García, *J. Am. Chem. Soc.* **2011**, *133*, 595–602; b) H. Li, Z. Bian, J. Zhu, Y. Huo, H. Li, Y. Lu, *J. Am. Chem. Soc.* **2007**, *129*, 4538–4539.
[6] a) K. Qian, B. C. Sweeny, A. C. Johnston-Peck, W. Niu, J. O. Graham, J. S. DuChene, J. Qiu, Y.-C. Wang, M. H. Engelhard, D. Su, *J. Am. Chem. Soc.* **2014**, *136*, 9842–9845; b) V. Subramanian, E. E. Wolf, P. V. Kamat, *J. Am. Chem. Soc.* **2004**, *126*, 4943–4950; c) N. Wang, T. Tachikawa, T. Majima, *Chem. Sci.* **2011**, *2*, 891–900; d) F. Amano, E. Ishinaga, A. Yamakata, *J. Phys. Chem. C* **2013**, *117*, 22584–22590.
[7] a) T. Schaaff, D. Blom, *Nano Lett.* **2002**, *2*, 507–511; b) D. R. Rolison, *Science* **2003**, *299*, 1698–1701; c) A. T. Bell, *Science* **2003**, *299*, 1688–1691.
[8] a) Z. Jin, M. Xiao, Z. Bao, P. Wang, J. Wang, *Angew. Chem. Int. Ed.* **2012**, *51*, 6406–6410; *Angew. Chem.* **2012**, *124*, 6512–6516; b) A. Tanaka, K. Hashimoto, H. Kominami, *J. Am. Chem. Soc.* **2012**, *134*, 14526–14533.
[9] a) Y. Li, W. Luo, N. Qin, J. Dong, J. Wei, W. Li, S. Feng, J. Chen, J. Xu, A. A. Elzatahry, M. H. Es-Saheb, Y. Deng, D. Zhao, *Angew. Chem. Int. Ed.* **2014**, *53*, 9035–9040; *Angew. Chem.* **2014**, *126*, 9181–9186; b) J. Lee, M. C. Orilall, S. C. Warren, M. Kamperman, F. J. DiSalvo, U. Wiesner, *Nat. Mater.* **2008**, *7*, 222–228.
[10] J. He, Y. Liu, T. Babu, Z. Wei, Z. Nie, *J. Am. Chem. Soc.* **2012**, *134*, 11342–11345.
[11] a) J. J. Mock, D. R. Smith, S. Schultz, *Nano Lett.* **2003**, *3*, 485–491; b) S. Link, M. A. El-Sayed, *J. Phys. Chem. B* **1999**, *103*, 8410–8426.
[12] G. Wang, Y. Ling, H. Wang, X. Yang, C. Wang, J. Z. Zhang, Y. Li, *Energy Environ. Sci.* **2012**, *5*, 6180–6187.
[13] P. V. Kamat, *J. Phys. Chem. Lett.* **2012**, *3*, 663–672.
[14] C. Harris, P. V. Kamat, *Acs Nano* **2010**, *4*, 7321–7330.
[15] C. H. Kuo, W. Li, L. Pahalagedara, A. M. El-Sawy, D. Kriz, N. Genz, C. Guild, T. Ressler, S. L. Suib, J. He, *Angew. Chem. Int. Ed.* **2015**, *54*, 2345–2350; *Angew. Chem.* **2015**, *127*, 2375–2380.

Received: March 29, 2015
Revised: April 27, 2015
Published online: June 12, 2015

